

Revealing the non-adiabatic and non-Abelian multiple-band effects via anisotropic valley Hall conduction in bilayer graphene

Ci Li,^{1,2,*} Matisse Wei-Yuan Tu,^{3,†} and Wang Yao^{1,2}

¹*Department of Physics, The University of Hong Kong, Hong Kong, China*

²*HKU-UCAS Joint Institute of Theoretical and Computational Physics at Hong Kong, China*

³*Department of Physics, National Sun Yat-sen University, Taiwan*

Many quantum materials of interest, ex., bilayer graphene, possess a number of closely spaced but not fully degenerate bands near the Fermi level, where the coupling to the far detuned remote bands can induce Berry curvatures of the non-Abelian character in this active multiple-band manifold for transport effects. Under finite electric fields, non-adiabatic interband transition processes are expected to play significant roles in the associated Hall conduction. Here through an exemplified study on the valley Hall conduction in AB-stacked bilayer graphene, we show that the contribution arising from non-adiabatic transitions around the bands near the Fermi energy to the Hall current is not only quantitatively about an order-of-magnitude larger than the contribution due to adiabatic inter-manifold transition with the non-Abelian Berry curvatures. Due to the trigonal warping, the former also displays an anisotropic response to the orientation of the applied electric field that is qualitatively distinct from that of the latter. We further show that these anisotropic responses also reveal the essential differences between the diagonal and off-diagonal elements of the non-Abelian Berry curvature matrix in terms of their contributions to the Hall currents. We provide a physically intuitive understanding on the origin of distinct anisotropic features from different Hall current contributions, in terms of band occupations and interband coherence. This then points to the generalization beyond the specific example of bilayer graphenes.

I. INTRODUCTION

Band structure effects on transport of electrons driven by an external electric field constitute one of the most fundamental issues in solid-state physics¹. In principle, one can group the electronic bands into two kinds of manifolds, namely, the active and the remote, according to the relation between the relevant gaps and the applied field. The active manifold contains those bands around the Fermi energy which play the dominant roles in the field-driven transport. Other bands are categorised into the remote manifold. Due to the relatively large gaps between the active and the remote manifolds, the field-induced inter-manifold transitions are well captured by the adiabatic approximation, in which the electric field is treated as a perturbation. When the active manifold contains a single band or a number of fully degenerate bands, this adiabatic description has been successful in manifesting one of the most non-trivial band structure effects on electron transport, namely, the Hall effect²⁻⁸, which includes a number of varieties such as spin⁹⁻¹² and valley Hall effects^{13,14}. On the other hand, when the active manifold contains a number of closely spaced but not fully degenerate bands, the effects of a finite electric field on the interband transitions within the active manifold are beyond the validity of perturbation treatment and therefore also requires non-adiabatic consideration. Correspondingly, this leads to a non-adiabatic Hall effect, which has been found to be pronounced in Dirac cones with a Berry curvature hotspot, as recently discussed¹⁵ and extended to situations with spatially varied band structures¹⁶.

Although previous studies have respectively expounded on the Hall effects in the adiabatic regime

and expanded into the non-adiabatic one, interesting realistic materials such as transition metal dichalcogenides (ex. twisted MoSe₂ homobilayers¹⁷⁻²⁰) and bilayer graphenes²¹ indeed possess band structures that demand a coherent unification of the above two perspectives. Explicitly, from the view of the carrier motion, the Hall effect is rooted to the anomalous part of the velocity. On one end, when the active manifold contains only a single band or fully degenerate bands over the whole Brillouin zone, the adiabatic inter-manifold transition results in the well-known expression of the anomalous velocity in terms of the Berry curvatures of the active bands^{5,8,16,22,23}. On the other end, when the remote bands are completely ignored, non-adiabatic dynamics among the non-degenerate bands within the active manifold gives rise to a renormalized carrier velocity due to the finite electric field, that also has an anomalous part contributing to the corresponding non-adiabatic Hall effect¹⁵. Naturally, the consequence from the interplay of these two ends is an important question worthy further investigation, since many quantum materials of interest do have non-degenerate active bands together with non-negligible coupling to remote bands.

Apart from the non-adiabatic effects mentioned above, the multiple-band nature of the active manifold, as well-known, also gives rise to the non-Abelian characters of Berry curvatures upon projecting out the remote bands⁸ (see also¹⁶ for pedagogical derivation). On one hand, from the current response to an infinitesimal applied field, the pure geometrical aspects of the non-Abelian characters on the Hall currents have been well understood^{10,24}. On the other hand, the non-Abelian Berry curvatures as anomalous driving forces for the dynamics of single wave packets have also been anal-

ysed through the peculiarly induced motion under various contexts^{25–28}. Nevertheless, the interplay between these two faces of multiple-band effects, namely, the non-Abelian characters and the non-adiabatic dynamics still remains an open question.

In this work, we address the above raised issues through investigating the valley Hall currents in biased graphene bilayer with a modest gap (0.01eV) (Fig. 1(a))^{21,29–37}. The effective four-band model for this material features two bands close in energy forming the active manifold and two other remote bands separated from the active bands by around 0.4eV (see Fig. 1(b)), suitable for the present purpose.

Explicitly, we investigate the transverse valley currents of *AB*-stacked bilayer graphene under finite external electric fields. We treat both the contributions from the adiabatic inter-manifold-transitions and non-adiabatic intra-active-manifold transitions to the Hall conduction on an equal footing. The main point of the present research is to establish that the non-adiabatic aspect of the Hall current is a distinct facet that is qualitatively different from the more familiar Hall effect usually studied in the adiabatic regime. This is revealed through the dependence of the Hall current on the angle between the applied electric field and the crystalline axis, exploiting the anisotropy from trigonal warping of the electronic band structure of *AB*-stacked bilayer graphene. The ability to apply an electric field along various directions across a sample has been experimentally realized³⁸ with an attempt to facilitate the study of the well-known nonlinear Hall effect supported by *Abelian* Berry curvature dipoles³⁹. We show that the feasibility on the angular-dependence of the Hall current not only reveals the crucial distinctions between the adiabatic inter-manifold and the non-adiabatic intra-active-manifold contributions to the Hall current. But it also uncovers interesting difference between contributions involving diagonals and off-diagonals from the *non-Abelian* Berry curvatures matrix.

II. UNIFIED DESCRIPTION OF ADIABATIC AND NON-ADIABATIC REGIMES

To begin, we first summarise the main framework that unify the wave-packet description of electronic transport for both the adiabatic and the non-adiabatic regimes¹⁶. We consider a general band structure, described by the Hamiltonian, $\mathcal{H}(\mathbf{k})$ that totally has N_A bands in the active manifold A and N_R bands in the remote manifold R . The band wavefunctions and energies of $\mathcal{H}(\mathbf{k})$ are denoted respectively by $|u_n(\mathbf{k})\rangle$ and $\varepsilon_n(\mathbf{k})$ with the band index n and the Bloch wave vector \mathbf{k} . The separation between the manifolds A and R means $\forall n_a, m_a \in A$ and $\forall n_r \in R$ that

$$|\varepsilon_{n_a} - \varepsilon_{n_r}| \gg \text{MAX}_{m \in A} |\varepsilon_{n_a} - \varepsilon_m|, \quad \frac{|\varepsilon_{n_a} - \varepsilon_{n_r}|}{|\varepsilon_{m_a} - \varepsilon_{n_r}|} \approx 1,$$

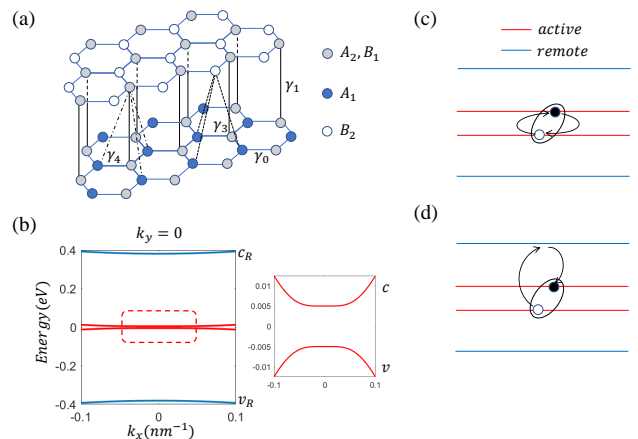


FIG. 1. (Color online) (a): The atomic structure of an *AB*-stacked bilayer graphene in side view. (b): The four-band dispersion (with $\gamma_3 = 0$ in (a), see also Eq. (8)) clearly distinguishing the active and the remote bands. (c): Interband coherence directly formed through non-adiabatic intra-active-manifold dynamics. (d): Interband coherence indirectly formed through adiabatic inter-manifold transitions. They imply distinct roles in their respective contributions to the Hall conduction.

The dynamics of a single wave packet is described by the time dependent Schrödinger equation $i\hbar|\dot{u}(t)\rangle = \mathcal{H}(\mathbf{k})|u(t)\rangle$ in which the carrier's Bloch wave vector acquires its time dependence $\hbar\dot{\mathbf{k}} = -e\mathbf{E}$ through the driving of an external electric field \mathbf{E} . The solution has the form $|u(t)\rangle = \sum_{n \in A+R} \eta_n(t) e^{i\gamma_n(\mathbf{k})} |u_n(\mathbf{k})\rangle$ with the band amplitudes η_n subject to normalisation. Here $\gamma_n(\mathbf{k}) = \int_{\mathbf{k}_0}^{\mathbf{k}} d\mathbf{k}' \cdot [\mathcal{R}_{\mathbf{k}'}]_{n,n}$ is the Berry phase of band n for a trajectory of \mathbf{k} starting from \mathbf{k}_0 and $[\mathcal{R}_{\mathbf{k}}]_{n,m} = i\langle u_n | \frac{\partial}{\partial \mathbf{k}} | u_m \rangle$ denotes the Berry connection between bands n and m .

By projecting out the remote bands while retaining their effects, the centre-of-mass motion of a single wave packet is described by the following equations,

$$\dot{\mathbf{r}} = \left\langle [D_{\hbar\mathbf{k}}, \mathcal{H}_A(\mathbf{k})] - \dot{\mathbf{k}} \times \mathcal{F}_{\mathbf{k}} \right\rangle_A, \quad (1a)$$

$$\hbar\dot{\mathbf{k}} = -e\mathbf{E} \quad (1b)$$

where $\mathcal{H}_A(\mathbf{k})$ denotes the projection of $\mathcal{H}(\mathbf{k})$ into the active manifold and

$$[D_{\mathbf{k}}]_{n,m} = \delta_{n,m} \frac{\partial}{\partial \mathbf{k}} - i[\mathcal{R}_{\mathbf{k}}]_{n,m}, \quad (1c)$$

is the covariant derivative. The boldface $\mathcal{F}_{\mathbf{k}}$ stands for a rank-1 tensor as a vector whose spatial components $\mathcal{F}_{\mathbf{k}}^\lambda$'s are related to the rank-2 Berry curvature tensor $(1/2)\epsilon^{\alpha\beta\lambda} [\mathcal{F}_{\mathbf{k}}^{\alpha\beta}] = \mathcal{F}_{\mathbf{k}}^\lambda$ where $\epsilon^{\alpha\beta\lambda}$ is the Levi-Civita symbol and

$$\mathcal{F}_{\mathbf{k}}^{\alpha\beta} = \left\{ \frac{\partial [\mathcal{R}_{k_\beta}]}{\partial k_\alpha} - \frac{\partial [\mathcal{R}_{k_\alpha}]}{\partial k_\beta} - i[\mathcal{R}_{k_\alpha}, \mathcal{R}_{k_\beta}] \right\}, \quad (1d)$$

which retains the non-Abelian matrix structure of the Berry connections $\mathcal{R}_{\mathbf{k}}$ in band indices. Here the square bracket stands for the average $\langle O \rangle_A = \sum_{n,m \in A} \eta_n^* O_{n,m} \eta_m$ over the band amplitudes η_m 's, which are subject to

$$i\hbar\dot{\boldsymbol{\eta}} = \bar{\mathcal{H}}\boldsymbol{\eta} \quad (2a)$$

where the matrix elements of the moving-frame Hamiltonian $\bar{\mathcal{H}}$ read

$$\bar{\mathcal{H}}_{n,m} = \delta_{n,m}\varepsilon_n + (1 - \delta_{n,m})e\mathbf{E} \cdot [\bar{\mathcal{R}}_{\mathbf{k}}]_{n,m}, \quad (2b)$$

in which $[\bar{\mathcal{R}}_{\mathbf{k}}]_{n,m} = e^{-i\gamma_n} [\mathcal{R}_{\mathbf{k}}]_{n,m} e^{i\gamma_m}$. The non-Abelian Berry curvature $\mathcal{F}_{\mathbf{k}}^{\alpha\beta}$ given by Eq. (1d) arises from adiabatic inter-manifold transitions and is independent of \mathbf{E} . Nevertheless, its influences on the carrier velocity $\dot{\mathbf{r}}$, manifested through the second term in Eq. (1a), namely, $\langle \mathcal{F}_{\mathbf{k}} \rangle_A$, contains the non-adiabatic intra-active-manifold dynamics embedded in $\boldsymbol{\eta}$ that displays non-perturbation effects from a finite \mathbf{E} (see Eq. (2)).

The electrical currents arise from an ensemble of wave packets. By taking into accounts the scattering effects and the decoherence within the band space¹⁶, the electric current is found to be

$$\mathbf{J} = -e \sum_i \int_{\mathbf{k}} g_i(\mathbf{k}) \bar{\mathbf{v}}_i(\mathbf{k}), \quad (3a)$$

where we have abbreviated $\int d\mathbf{k}$ by $\int_{\mathbf{k}}$. Here $\bar{\mathbf{v}}_i$ is the ensemble-averaged velocity, containing two contributions,

$$\bar{\mathbf{v}}_i = \bar{\mathbf{v}}_i^A + \bar{\mathbf{v}}_i^R. \quad (3b)$$

The intra-active-manifold non-adiabatic dynamics contributes with

$$\bar{\mathbf{v}}_i^A = \bar{\mathbf{v}}_i^{\text{occ},A} + \bar{\mathbf{v}}_i^{\text{coh},A} \quad (4a)$$

where

$$\bar{\mathbf{v}}_i^{\text{occ},A} = \sum_{n \in A} |\bar{\eta}_n^i|^2 \frac{\partial \varepsilon_n}{\partial \mathbf{k}}, \quad (4b)$$

is the normal velocity due to band dispersion and

$$\bar{\mathbf{v}}_i^{\text{coh},A} = \sum_{n \neq m \in A} (\bar{\eta}_n^i)^* \left[\frac{\partial \mathcal{H}_A}{\partial \hbar \mathbf{k}} \right]_{n,m} \bar{\eta}_m^i, \quad (4c)$$

is one part of the anomalous velocity. The other part of the anomalous velocity is contributed by the inter-manifold adiabatic dynamics with

$$\bar{\mathbf{v}}_i^R = \bar{\mathbf{v}}_i^{\text{occ},R} + \bar{\mathbf{v}}_i^{\text{coh},R}, \quad (5a)$$

where

$$\bar{\mathbf{v}}_i^{\text{occ},R} = \frac{e}{\hbar} \mathbf{E} \times \sum_{n \in A} |\bar{\eta}_n^i|^2 [\mathcal{F}_{\mathbf{k}}]_{n,n}, \quad (5b)$$

and

$$\bar{\mathbf{v}}_i^{\text{coh},R} = \frac{e}{\hbar} \mathbf{E} \times \sum_{n \neq m \in A} (\bar{\eta}_n^i)^* [\mathcal{F}_{\mathbf{k}}]_{n,m} \bar{\eta}_m^i. \quad (5c)$$

come from projecting the inter-manifold dynamics onto the band occupations $|\bar{\eta}_n^i|^2$ and interband coherence $(\bar{\eta}_n^i)^* \bar{\eta}_m^i$ in the active manifold respectively. Here $\bar{\boldsymbol{\eta}}^i$, a vector with components $\bar{\eta}_n^i$ enumerated by n , is defined as an eigenvector of the moving-frame Hamiltonian's projection on active bands, $\bar{\mathcal{H}}_A(\mathbf{k}, \mathbf{E})$, indexed with i , namely, $\bar{\mathcal{H}}_A \bar{\boldsymbol{\eta}}^i = \mathcal{E}_i \bar{\boldsymbol{\eta}}^i$ with \mathcal{E}_i the corresponding eigenvalue. We call $\bar{\boldsymbol{\eta}}^i$'s the hybridised bands and they depend on the electric field in a non-perturbation way^{15,16}. The physical meaning is the following. The joint action of decoherence and the electric field favours a certain form of interband coherence as those contained in $\bar{\boldsymbol{\eta}}^i$'s. As a result, the carriers are led to a statistical mixture of the hybridised bands $\bar{\boldsymbol{\eta}}^i$'s. The distribution function with respect to occupations on the hybridised bands is given by $g_i = g_i^0 + \delta g_i$ where $g_i^0 = 1 / \left[\exp\left(\frac{\mathcal{E}_i - \mu}{k_B T}\right) + 1 \right]$ with μ the chemical potential and T the temperature and $\delta g_i = (e/\hbar) \tau \mathbf{E} \cdot \partial g_i^0 / \partial \mathbf{k}$ with τ the relaxation time⁴².

The current Eq. (3) can be further decomposed as

$$\mathbf{J} = \mathbf{J}^L + \mathbf{J}^H,$$

where $\mathbf{J}^L = -e \int_{\mathbf{k}} \sum_i \delta g_i \bar{\mathbf{v}}_i$ and

$$\mathbf{J}^H = \mathbf{J}_A^H + \mathbf{J}_R^H, \quad (6a)$$

in which

$$\mathbf{J}_A^H = -e \int_{\mathbf{k}} \sum_i g_i^0 \bar{\mathbf{v}}_i^{\text{coh},A}, \quad \mathbf{J}_R^H = -e \int_{\mathbf{k}} \sum_i g_i^0 \bar{\mathbf{v}}_i^R \quad (6b)$$

on knowing that $\int_{\mathbf{k}} g_i^0 \bar{\mathbf{v}}_i^{\text{occ},A} = 0^1$. These two contributions \mathbf{J}^L and \mathbf{J}^H respectively reproduce the well-established expressions of the longitudinal current and the Hall current in the limit of infinitesimal \mathbf{E} ^{8,16}. In this work, we are only interested in \mathbf{J}^H .

Within this framework, the issues raised in the introduction can now be addressed. The first question is on the interplay between the respective contributions to the Hall current arising from adiabatic coupling to remote bands and from non-adiabatic dynamics within the active manifold. This can be approached from the well-known notion that the Hall current is mediated by the interband coherence⁷. Both contributions \mathbf{J}_A^H and \mathbf{J}_R^H contain interband coherence among the active bands, namely, $(\bar{\eta}_n^i)^* \bar{\eta}_m^i$ for $n \neq m$ with $n, m \in A$. Such coherence in \mathbf{J}_A^H explicated by Eq. (4c) is directly formed through the field-induced interband transitions within the active manifold. In contrast, for \mathbf{J}_R^H , such coherence given by Eq. (5c) is only indirectly formed through transitions forth and back between the active and the remote bands (see illustrations in Fig. 1(c) and (d) respectively). This leads us to anticipate that the natures of the Hall current manifested via \mathbf{J}_A^H and \mathbf{J}_R^H can be very different.

The second question concerns the two faces of the multiple-band effects, namely, the non-adiabatic dynamics and the non-Abelian characters of the Berry curvatures. This can be viewed from the decomposition

$$\mathbf{J}_R^H = \mathbf{J}_{\text{occ},R}^H + \mathbf{J}_{\text{coh},R}^H, \quad (7a)$$

where

$$\mathbf{J}_{\text{occ/coh},R}^H = -e \int_{\mathbf{k}} \sum_i g_i^0 \bar{\mathbf{v}}_i^{\text{occ/coh},R}. \quad (7b)$$

When the active bands are fully degenerate over the Brillouin zone, $\mathbf{J}_{\text{coh},R}^H$ has no contribution to the Hall current, as we have discussed in Ref.¹⁶. There we have also shown that the Hall current reduces to the well-established expression $\mathbf{J}^H = (e^2/\hbar) \mathbf{E} \times \int_{\mathbf{k}} \text{Tr}(\mathcal{F}_{\mathbf{k}})$ ²⁴ when the degenerate band energy is set below the Fermi energy. The gauge symmetry associated with band degeneracy can be utilized to study the non-Abelian characters⁴³. For general non-degenerate bands, where gauge symmetry is not expected, the non-Abelian characters of $\mathcal{F}_{\mathbf{k}}^z$ as matrices are fully embedded in the decomposition Eq. (7). In conjunction with Eq. (5), we find the two current contributions $\mathbf{J}_{\text{occ},R}^H$ and $\mathbf{J}_{\text{coh},R}^H$ involve only the diagonals and the off-diagonals of $\mathcal{F}_{\mathbf{k}}^z$ respectively, bearing also distinct physical meanings as currents arising from band occupations and interband coherence. Comparison between $\mathbf{J}_{\text{occ},R}^H$ and $\mathbf{J}_{\text{coh},R}^H$ thus provides a mean to reveal the multiple-band effects that underlie the Hall currents including both the non-Abelian characters of $\mathcal{F}_{\mathbf{k}}^z$ and non-adiabatic effects embedded in $\bar{\eta}_n^i$'s. In the following, we illustrate these points in *AB*-stacked bilayer graphenes.

III. THE BAND MANIFOLDS OF *AB*-STACKED BILAYER GRAPHENE

The energy dispersion relation, including both active and remote manifolds, for *AB*-stacked bilayer graphene can be analytically obtained. In the basis of the sublattices of the two layers 1 and 2, labeled as A_1, B_1, A_2, B_2 (see Fig. 1(a)), the effective four-band Hamiltonian near the Dirac point K (or K') can be expressed as²¹

$$\mathcal{H}(\mathbf{k}) = \begin{pmatrix} \epsilon_{A_1} & f\pi^\dagger & -f_4\pi^\dagger & f_3\pi \\ f\pi & \epsilon_{B_1} & \gamma_1 & -f_4\pi^\dagger \\ -f_4\pi & \gamma_1 & \epsilon_{A_2} & f\pi^\dagger \\ f_3\pi^\dagger & -f_4\pi & f\pi & \epsilon_{B_2} \end{pmatrix} \quad (8)$$

with $\pi = \xi k_x + ik_y$, $f = \sqrt{3}a\gamma_0/2$, and $f_{3,4} = \sqrt{3}a\gamma_{3,4}/2$ in which $\xi = \pm 1$ is the valley index and a is the lattice constant. The on-site potentials can be represented explicitly as $\epsilon_{A_1} = -\frac{1}{2}U$, $\epsilon_{B_1} = \frac{1}{2}(-U + 2\Delta')$, $\epsilon_{A_2} = \frac{1}{2}(U + 2\Delta')$, and $\epsilon_{B_2} = \frac{1}{2}(U - \delta_{AB})$, with U the interlayer asymmetry between the two layers, Δ' for an energy difference between dimer and non-dimer sites. The intralayer hopping between the A and B sites is given

by γ_0 and the meanings of various interlayer couplings γ_i with $i = 1, 3, 4$ are indicated in Fig. 1(a). Following Ref.⁴⁵, we fix $a = 2.46\text{\AA}$, $\gamma_0 = 3.16\text{eV}$, $\gamma_1 = 0.381\text{eV}$ and $\gamma_4 = \Delta' = 0$ throughout this work.

The band energies obtained from diagonalising Eq. (8) is illustrated in Fig. 1(b) clearly show two bands around the Fermi energy. They are the lowest conduction band and the highest valence band, indexed by c and v respectively, that form the active manifold. The remote bands consist of the higher conduction band c_R and the lower valence band v_R (see Fig. 1(b)). The valley Hall current is $\mathbf{J}^H = \mathbf{J}_A^H + \mathbf{J}_R^H$ detailed in Eq. (6). By Eqs. (6b) and (5), we see \mathbf{J}_R^H is perpendicular to \mathbf{E} . As shown in an earlier study that for active manifolds with two bands, \mathbf{J}_A^H is also perpendicular to \mathbf{E} ¹⁵. We apply the polar coordinate, i.e., $\mathbf{E} = E\hat{\rho}$ with the basis vector $\hat{\rho} = \hat{x} \cos \theta + \hat{y} \sin \theta$ and $\hat{\theta} = -\hat{x} \sin \theta + \hat{y} \cos \theta$. Here $E \equiv |\mathbf{E}|$ and θ is the angle between \mathbf{E} and \hat{x} . It is then sufficient to investigate the scalars $J_{A/R}^H = \hat{\theta} \cdot \mathbf{J}_{A/R}^H$ and $J_{\text{occ/coh},R}^H = \hat{\theta} \cdot \mathbf{J}_{\text{occ/coh},R}^H$. For definiteness, we place the chemical potential μ in the middle of the gap. Then only the lower-energy hybridised band, indexed by i_v , needs to be counted at very low temperatures in \sum_i in Eq. (6b). This simplifies $J_{\text{occ/coh},R}^H = -e \int_{\mathbf{k}} \bar{v}_{i_v}^{\text{occ/coh},R}$ with $\bar{v}_{i_v}^{\text{occ/coh},R} = \hat{\theta} \cdot \bar{\mathbf{v}}_{i_v}^{\text{occ/coh},R}$ (see Eqs. (5) and (6)) and $J_A^H = -e \int_{\mathbf{k}} \bar{v}_{i_v}^{\text{coh},A}$ with $\bar{v}_{i_v}^{\text{coh},A} = \hat{\theta} \cdot \bar{\mathbf{v}}_{i_v}^{\text{coh},A}$ (see Eqs. (4) and (6)).

IV. INTRA- VERSUS INTER-MANIFOLD CONTRIBUTIONS TO THE HALL CURRENTS

Since $\mathbf{E} = E\hat{\rho}(\theta)$ is a vector, $J_{A/R}^H$ in principle depends on both E and θ . When the dispersion of the system is isotropic, then the dependence of J^H on θ disappears. The two contributions J_A^H and J_R^H should depend on E very distinctively. When the dispersion is anisotropic, then J_A^H and J_R^H should also depend on θ , which characterises the orientation of the applied field, in very different manners. We now discuss explicitly how these are revealed.

The isotropy of dispersion here for the *AB*-stacked bilayer graphenes is determined by γ_3 , an interlayer skew hopping parameter (see Fig. 1(a)). With $\gamma_3 = 0$, the distinction between J_A^H and J_R^H is simply displayed in the order-of-magnitude difference between the current values, plotted as functions of E in Fig. 2(a) in unit of E_0 ⁴⁴. By defining

$$r_{n,m}(\mathbf{k}, \mathbf{E}) = \left| \frac{[\bar{\mathcal{R}}_{\mathbf{k}}]_{n,m} \cdot e\mathbf{E}}{\epsilon_n - \epsilon_m} \right| \quad (9)$$

as a dimensionless quantity that measures the ratio between the field-induced interband coupling to the gap size¹⁵ at a given \mathbf{k} , E_0 is the field strength that satisfies $\text{MAX } r_{c,v}(\mathbf{k}, E_0) = 1$. One can calculate J^H by the full-band formulation discussed in Ref.¹⁶, without separating

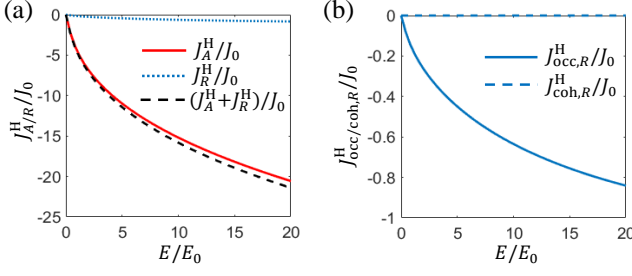


FIG. 2. (Color online) Under isotropic dispersion with $\gamma_3 = 0$, different contributions to the Hall currents only depend on the magnitude E of applied field \mathbf{E} . (a): The non-adiabatic intra-manifold contribution J_A^H and adiabatic inter-manifold contribution J_R^H show significant quantitative difference. (b): The two components $J_{\text{occ},R}^H$ and $J_{\text{coh},R}^H$ in Eq. (7a). Under such isotropic dispersion, only the diagonals of the non-Abelian matrix are involved in the nonzero contribution $J_{\text{occ},R}^H$ to J_R^H . Here the currents are in unit of $J_0 = e^2 E_0/h$, where $E_0 = 1.15\text{V}/\mu\text{m}$ is chosen such that $\text{MAX } r_{c,v}(\mathbf{k}, E_0) = 1$ (see Eq. (9)). The energy gap is $U = 0.01\text{eV}$.

the contributions into J_A^H and J_R^H . We have verified that the computations here based on Eq. (6) agree with the results of full-band calculation. The consistency with full-band calculation signifies that it indeed makes sense to simultaneously speak of the adiabatic contribution (from coupling to remote band), and the non-adiabatic contribution (from intra-manifold coupling) to the Hall effect over a sizable range of the electric field. In addition, under the condition $\gamma_3 = 0$, we found that J_R^H is entirely dominated by $J_{\text{occ},R}^H$ with vanishing contribution from $J_{\text{coh},R}^H$ (see Fig. 2b)). We will show that when $\gamma_3 \neq 0$, more interesting differences between $J_{\text{occ},R}^H$ and $J_{\text{coh},R}^H$ can arise.

When $\gamma_3 \neq 0$ the anisotropy of the dispersion appears (see Fig. 3(a)), allowing non-trivial θ -dependence of $J_R^H = J_{\text{occ},R}^H + J_{\text{coh},R}^H$ and J_A^H . From Eqs. (7) and (5), we see on one hand, $J_{\text{occ},R}^H$ depends on θ through the band occupations $|\bar{\eta}_c^{i_v}|^2$ and $|\bar{\eta}_v^{i_v}|^2$ that have the same period in θ in $\bar{v}_{i_v}^{\text{occ},R}$. On the other hand, $J_{\text{coh},R}^H$ gains θ -dependence through the interband coherence $(\bar{\eta}_c^{i_v})^* \bar{\eta}_v^{i_v}$ in $\bar{v}_{i_v}^{\text{coh},R}$. Explicitly, we have

$$|\bar{\eta}_c^{i_v}|^2 = \frac{1 \mp \varepsilon_g/\bar{\varepsilon}_g}{2}, \quad (\bar{\eta}_c^{i_v})^* \bar{\eta}_v^{i_v} = -\frac{[\bar{\mathcal{R}}_{\mathbf{k}}]_{v,c} \cdot \mathbf{E}}{\bar{\varepsilon}_g} \quad (10)$$

where $\varepsilon_g = \varepsilon_c - \varepsilon_v$ and

$$\bar{\varepsilon}_g = \sqrt{\varepsilon_g^2 + 4 \left| [\bar{\mathcal{R}}_{\mathbf{k}}]_{v,c} \cdot \mathbf{E} \right|^2} \quad (11)$$

is the renormalized gap. Using $\mathbf{E} = E(\hat{x} \cos \theta + \hat{y} \sin \theta)$, we straightforwardly see that $(\bar{\eta}_c^{i_v})^* \bar{\eta}_v^{i_v}$ has a θ -period that is twice of that of $|\bar{\eta}_c^{i_v}|^2$ and $|\bar{\eta}_v^{i_v}|^2$. So the θ -period of J_R^H is led by that of $J_{\text{coh},R}^H$, which is associated with the interband coherence that appears in $\bar{v}_{i_v}^{\text{coh},R}$ of Eq. (5).

We now turn to the θ -dependence in J_A^H . From Eqs. (6) and (4), we find that J_A^H depends on θ through the term $(\bar{\eta}_c^{i_v})^* \bar{\eta}_v^{i_v} \hat{\theta} \cdot \partial \mathcal{H}_A / \partial \hbar \mathbf{k}$ that appears in $\bar{v}_{i_v}^{\text{coh},A}$. Here $\hat{\theta} \cdot \partial \mathcal{H}_A / \partial \hbar \mathbf{k} = (-\sin \theta \partial \mathcal{H}_A / \partial \hbar k_x + \cos \theta \partial \mathcal{H}_A / \partial \hbar k_y)$ which makes the θ -period of $(\bar{\eta}_c^{i_v})^* \bar{\eta}_v^{i_v} \hat{\theta} \cdot \partial \mathcal{H}_A / \partial \hbar \mathbf{k}$ only half as that of $(\bar{\eta}_c^{i_v})^* \bar{\eta}_v^{i_v}$. These two different θ -dependencies, namely, $(\bar{\eta}_c^{i_v})^* \bar{\eta}_v^{i_v}$ and $(\bar{\eta}_c^{i_v})^* \bar{\eta}_v^{i_v} \hat{\theta} \cdot \partial \mathcal{H}_A / \partial \hbar \mathbf{k}$, are revealed correspondingly in the velocities $\bar{v}_{i_v}^{\text{coh},R}$ and $\bar{v}_{i_v}^{\text{coh},A}$, plotted as functions of θ in Fig. 3(b) and (c) respectively. It clearly shows the distinctively different periods.

From the above analysis with also the aids of Eqs. (5) and (4), the θ -period of the average carrier velocity $\bar{v}_{i_v}^{\text{coh},R}$ is twice as that of $\bar{v}_{i_v}^{\text{coh},A}$ at arbitrary \mathbf{k} regardless of the dispersion is anisotropic or isotropic. The currents are obtained by integrating the average carrier velocity over \mathbf{k} . The above discussed θ -period difference between $\bar{v}_{i_v}^{\text{coh},R}$ and $\bar{v}_{i_v}^{\text{coh},A}$ appears also in the difference between J_R^H and J_A^H only when the dispersion of the system is anisotropic. With $\gamma_3 \neq 0$, which leads to a well-known trigonal-warped dispersion^{21,46}, we show in Fig. 4(a) at a given valley $\xi = 1$ both current contributions J_R^H and J_A^H . It clearly shows that while J_R^H follows the C_3 symmetry of the energy dispersion, J_A^H exhibits C_6 symmetry. The θ -period of the current is different from the \mathbf{k} -resolved average carrier velocity due to integration over \mathbf{k} , which manifests the symmetry of the dispersion. Nevertheless, the character that $\bar{v}_{i_v}^{\text{coh},R}$ has its θ -period twice as that of $\bar{v}_{i_v}^{\text{coh},A}$ is fully revealed in the physical observable that J_R^H 's θ -period is twice of J_A^H 's. The intuitively anticipated qualitative difference between J_A^H and J_R^H from Fig. 1(c) and (d) is thus concretely illustrated through different periods in θ .

V. TWO FACES OF MULTIPLE-BAND EFFECTS: NON-ADIABATIC AND NON-ABELIAN

A. revelation on the Hall currents

We now focus on the remote band contribution J_R^H to reveal the relation between the underlying non-adiabatic dynamics and the non-Abelian characters raised from the multi-band effects in the active manifold. As we have mentioned before, when the active bands are fully degenerate and occupied, the linear conductivity is given by $\sigma^H = \partial J^H / \partial E|_{E=0} = (e^2/\hbar) \int_{\mathbf{k}} \text{Tr}(\mathcal{F}_{\mathbf{k}}^z)$, which depends neither on E nor on θ , as a consequence of its definition. Furthermore, this linear conductivity only involves the band diagonals of the Berry curvature matrix $\mathcal{F}_{\mathbf{k}}^z$.

As discussed before, anisotropy of the dispersion can be revealed in the Hall currents under the finite electric fields. In order to extract the θ -dependence more exclusively, we define $\Delta J_{\text{coh}/\text{occ},R}^H = J_{\text{coh}/\text{occ},R}^H - \bar{J}_{\text{coh}/\text{occ},R}^H$,

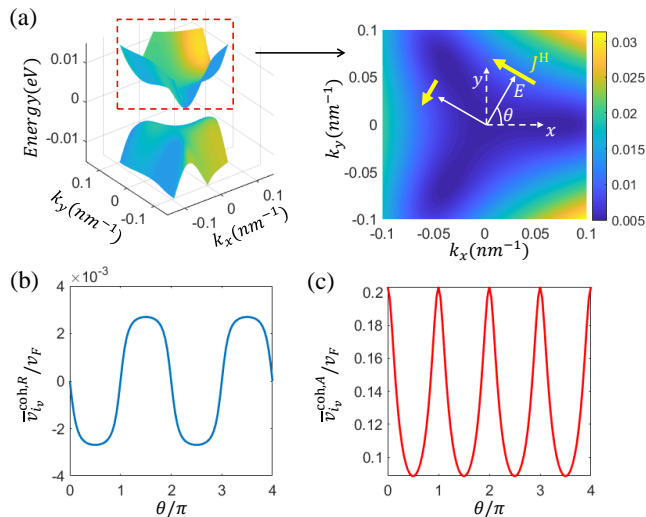


FIG. 3. (Color online) (a): The anisotropic dispersion of the bands near the Fermi energy, demonstrated with $\gamma_3 = 0.38\text{eV}^{45}$. Inset: The trigonal warping of active conduction band, implying that the magnitude of the Hall current (yellow arrows of different lengths) depends on the angle θ between \mathbf{E} (solid white arrows) and the crystal axis, here taken as \hat{x} (dashed white arrow). (b) and (c): Different θ -dependencies of the anomalous velocities $\bar{v}_{i_v}^{\text{coh},R}$ and $\bar{v}_{i_v}^{\text{coh},A}$ respectively, giving rise to distinct periods in θ and determining the anisotropic responses of J_R^H and J_A^H to θ (see the main text for details). The specific choice of \mathbf{k} is irrelevant. Here we use $k_x = 0.01\text{\AA}$ and $k_y = 0$. Other parameters follow that used in Fig. 2 with $E = E_0$ here and $v_F = \sqrt{3}a\gamma_0/\hbar$ as the Fermi velocity.

where we subtract the angular average $\bar{J}_{\text{coh/occ},R}^H = (1/\theta_T^{\text{coh/occ},R}) \int_0^{\theta_T^{\text{coh/occ},R}} d\theta J_{\text{coh/occ},R}^H$ in which $\theta_T^{\text{coh/occ},R}$ denotes the θ -period of $J_{\text{coh/occ},R}^H$. We plot $\Delta J_{\text{coh},R}^H$ (solid line) and $\Delta J_{\text{occ},R}^H$ (dashed line) as a function of θ in Fig. 4(b), which shows that $\theta_T^{\text{coh},R} = 2\theta_T^{\text{occ},R}$, as expected due to the reasons already discussed for Fig. 3. More interestingly, in Fig. 4(b) we see that $\Delta J_{\text{coh},R}^H$ displays a variation with respect to θ that is clearly greater than that of $\Delta J_{\text{occ},R}^H$. This is because the interband coherence $(\bar{\eta}_c^{i_v})^* \bar{\eta}_v^{i_v}$ in general is more sensitive to θ than the occupation $|\bar{\eta}_{c/v}^{i_v}|^2$ since the former is one order larger in $E \cos \theta$ and $E \sin \theta$ than the latter (see Eq. (10)). Note that in terms of $J_{\text{coh/occ},R}^H = \Delta J_{\text{coh/occ},R}^H + \bar{J}_{\text{coh/occ},R}^H$ we still have $J_{\text{occ},R}^H \gg J_{\text{coh},R}^H$ for $\gamma_3 \neq 0$. This is consistent with the observation in Fig. 2(b) where $\gamma_3 = 0$. Importantly, it is the anisotropy (sensitivity to θ 's variation due to $\gamma_3 \neq 0$) that pronounces the role of the off-diagonal term, due to which the Berry curvature is said to be non-Abelian. The underlying non-adiabatic dynamics, characterised by θ -dependence at finite \mathbf{E} , thus manifests the non-Abelian characters of $\mathcal{F}_{\mathbf{k}}^z$, differentiating between the diagonal $J_{\text{occ},R}^H$ and off-diagonal $J_{\text{coh},R}^H$ contributions.

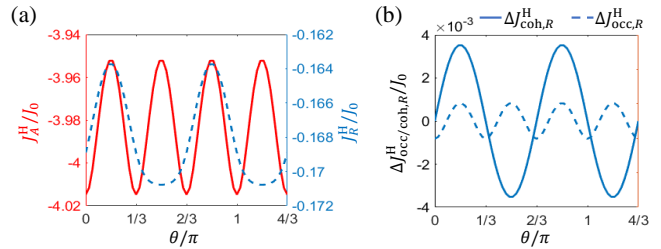


FIG. 4. (Color online) (a): The qualitative difference between J_R^H and J_A^H revealed through distinct symmetries (C_3 for J_R^H and C_6 for J_A^H). (b): Angular variations of inter-band coherence ($\Delta J_{\text{coh},R}^H$ as the solid line) and band-occupation ($\Delta J_{\text{occ},R}^H$ as the dashed line) contributions, respectively to the remote-band-mediated Hall current J_R^H , contrasting the diagonal and the off-diagonal involvements of the non-Abelian Berry curvature matrices. The parameters are same as what we take in Fig. 3 for both (b) and (c). The angular averages are $\bar{J}_{\text{occ},R}^H = 0.168J_0$ and $\bar{J}_{\text{coh},R}^H = 0$.

B. microscopic picture from \mathbf{k} -resolved processes

So far the two faces of multiple-band effects have been investigated through the \mathbf{k} -integrated currents. To have a deeper insight, we revisit the \mathbf{k} -resolved dimensionless quantity, Eq. (9). On one hand, with the band indices $n = c, m = v \in A$, Eq. (9) measures the strength of non-adiabatic intra-manifold transition with respect to the gap between active bands c and v . On the other hand, the underlying constituents of the non-Abelian Berry curvature Eq. (1d), which can be rewritten as $[\mathcal{F}_{\mathbf{k}}^{\alpha\beta}]_{(m',m) \in A} = \sum_{n \in R} \{i[\mathcal{R}_{k_\alpha}]_{m',n} [\mathcal{R}_{k_\beta}]_{n,m} - (k_\alpha \leftrightarrow k_\beta)\}$, are the inter-manifold Berry connections $[\mathcal{R}_{k_\beta}]_{n,m}$ contained in Eq. (9) with $n \in R$ and $m \in A$. We thus are able to explore the multiple-band effects from the \mathbf{k} -resolved information of Eq. (9).

In Fig. 5, we inspect \mathbf{k} -dependencies of $r_{c,v}(\mathbf{k}, \mathbf{E})$ (for non-adiabatic intra-active-manifold dynamics) and $r_{cR,v}(\mathbf{k}, \mathbf{E})$ (for constituents of non-Abelian Berry curvatures) respectively for both cases $\gamma_3 = 0$ and $\gamma_3 \neq 0$. The \mathbf{k} -dependence of $r_{c,v}$ follows the symmetry of \mathbf{k} -dependence of band energies $\varepsilon_{c/v}(\mathbf{k})$ (see Fig. 5(a) and (c) with respective energy dispersion in mind).⁴⁷ In contrast, $r_{cR,v}$ for $\gamma_3 = 0$ and that for $\gamma_3 \neq 0$ have similar patterns in \mathbf{k} -dependence (see Fig. 5(b) and (d)) that are distinct from the \mathbf{k} -dependence pattern of $r_{c,v}$'s in Fig. 5(a) and (c). Regardless of $\gamma_3 = 0$ or $\gamma_3 \neq 0$, $r_{cR,v}$'s do not follow the symmetry of energy dispersion in \mathbf{k} -dependence. This provides the insight that the non-adiabatic interband transitions and the transitions giving rise to non-Abelian Berry curvatures, where both are responsible for Hall currents, are fundamentally different in their natures.

As discussed before with an analysis of J^H 's dependence on \mathbf{E} 's orientation, such qualitative difference can be seen from \mathbf{k} -integrated currents only when the en-

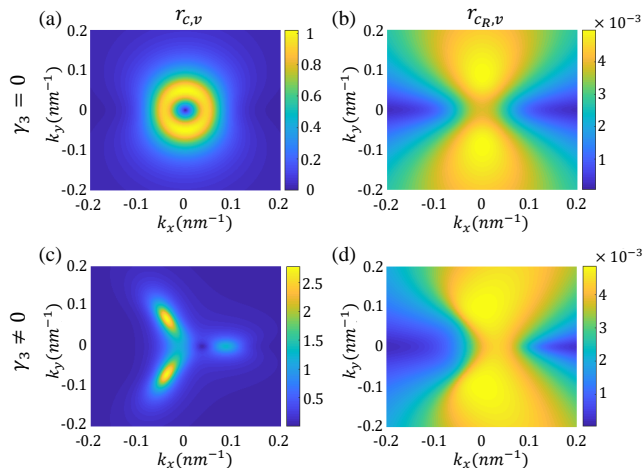


FIG. 5. (Color online) Visualization of the dimensionless non-adiabatic measure $r_{n,m}(\mathbf{k}, \mathbf{E} = E_0 \hat{x})$ in the \mathbf{k} -space for both isotropic ($\gamma_3 = 0$ as (a) and (b)) and anisotropic ($\gamma_3 = 0.38\text{eV}$ as (c) and (d)) dispersions. Other parameters are the same as in Fig. 2 (for $\gamma_3 = 0$) and Fig. 3 (for $\gamma_3 \neq 0$). Similarity between (b) and (d) is contrasted with dissimilarity between (a) and (c) to reveal the distinctness of non-adiabatic interband transitions as a multiple-band effect.

ergy dispersion is anisotropic. Crucially, even without energy anisotropy, the qualitative differences in the microscopic \mathbf{k} -resolved processes already underlie the origin that the non-adiabatic contribution to the Hall current is physically distinct from the adiabatic one, as a result of multiple-band effects.

VI. CONCLUSIONS AND DISCUSSIONS

In summary, through the studies of the valley Hall currents in typical *AB*-stacked bilayer graphenes as an example, we have demonstrated the followings. (i): The adiabatic inter-manifold contribution and the non-adiabatic intra-active-manifold contribution to the Hall current not only differ quantitatively about an order of magnitude due to the perturbation role of the electric field in the adiabatic inter-manifold transition processes. They also differ qualitatively in terms of the periodicity with respect to the angle of the applied electric field.

(ii): The non-Abelian characters due to the multiple-band nature of the active manifold are manifested by the difference between the diagonal and the off-diagonal contributions to the Hall current in terms not only of the periodicity with respect to the angle of the applied electric field but also of the angular variation amplitude.

The values of the angular periods and the shapes of the angular profiles for different contributions to the Hall currents depend on the details of the materials' electronic structures under consideration. Nevertheless, the conclusions (i) and (ii), confirmed by the calculations specifically designated to *AB*-stacked bilayer graphenes, are expected to be held also for other materials with anisotropic energy dispersion such that the Hall current at finite electric fields is sensitive to the orientation of the field. This is because the general analysis leading to the above conclusions is simply rooted to how band occupation and interband coherence differ fundamentally in their responses to the applied electric field (as exemplified for two-band active manifold in Eq. (10)). This fundamental difference also serves as the basis to manifest the multiple-band induced non-Abelian effects in Hall currents. Interestingly, this provides an intuitive approach toward the understanding of the non-Abelian characters, totally based on physically observable carrier transport currents, as complementary to the conventionally more mathematically oriented understanding based on quantum geometry of the band structures alone.

ACKNOWLEDGMENTS

C. Li would like to thank D. W. Zhai and B. Fu for useful discussions. The work is mainly supported by the Research Grants Council of Hong Kong (HKU17306819 and AoE/P-701/20), and the University of Hong Kong (Seed Funding for Strategic Interdisciplinary Research). M. W.-Y. Tu acknowledge the the hospitality of Prof. Tay-Rong Chang with support from ministry of technology and science in Taiwan of grand no. MOST110-2636-M-006-016. M. W.-Y. Tu also acknowledge the hospitality of National Center for Theoretical Science and thank Prof. Tse-Min Chen for useful discussions.

* oldsmith@hku.hk

† kerustemiro@gmail.com

¹ N. W. Ashcroft and N. D. Mermin, *Solid State Physics* (Sounders College, Philadelphia, 1976).

² R. Karplus and J. M. Luttinger, Hall effect in ferromagnetics, *Phys. Rev.* **95**, 1154 (1954).

³ J. M. Luttinger, Theory of the Hall effect in ferromagnetic substances, *Phys. Rev.* **112**, 739 (1958).

⁴ E. Adams and E. Blount, Energy bands in the presence of an external force field-II: Anomalous velocities, *J. Phys.*

Chem. Solids **10**, 286 (1959).

⁵ D. J. Thouless, M. Kohmoto, M. P. Nightingale, and M. D. Nijs, Quantized Hall Conductance in a Two-Dimensional Periodic Potential, *Phys. Rev. Lett.* **49**, 405 (1982).

⁶ T. Jungwirth, Q. Niu, and A. H. MacDonald, Anomalous Hall Effect in Ferromagnetic Semiconductors, *Phys. Rev. Lett.* **88**, 207208 (2002).

⁷ N. Nagaosa, J. Sinova, S. Onoda, A. H. MacDonald, and N. P. Ong, Anomalous Hall effect, *Rev. Mod. Phys.* **82**, 1539 (2010).

- ⁸ D. Xiao, M.-C. Chang, and Q. Niu, Berry phase effects on electronic properties, *Rev. Mod. Phys.* **82**, 1959 (2010).
- ⁹ S. Murakami, N. Nagaosa, and S.-C. Zhang, Dissipationless quantum spin current at room temperature, *Science* **301**, 1348 (2003).
- ¹⁰ S. Murakami, N. Nagaosa, and S. C. Zhang, *Phys. Rev. B* **69**, 235206 (2004).
- ¹¹ J. Sinova, D. Culcer, Q. Niu, N. A. Sinitsyn, T. Jungwirth, and A. H. MacDonald, Universal Intrinsic Spin Hall Effect, *Phys. Rev. Lett.* **92**, 126603 (2004).
- ¹² C. L. Kane and E. J. Mele, Z_2 Topological Order and the Quantum Spin Hall Effect, *Phys. Rev. Lett.* **95**, 146802 (2005).
- ¹³ D. Xiao, W. Yao, and Q. Niu, Valley-Contrasting Physics in Graphene: Magnetic Moment and Topological Transport, *Phys. Rev. Lett.* **99**, 236809 (2007).
- ¹⁴ D. Xiao, G.-B. Liu, W. Feng, X. Xu, and W. Yao, Coupled Spin and Valley Physics in Monolayers of MoS₂ and Other Group-VI Dichalcogenides, *Phys. Rev. Lett.* **108**, 196802 (2012).
- ¹⁵ M. W. Y. Tu, C. Li, H. Y. Yu, and W. Yao, Non-adiabatic Hall effect at Berry curvature hot spot, *2D Materials* **7**, 4 (2020).
- ¹⁶ M. W. Y. Tu, C. Li, and W. Yao, Theory of wave-packet transport under narrow gaps and spatial textures: Non-adiabaticity and semiclassicality, *Phys. Rev. B* **102**, 045423 (2020).
- ¹⁷ Y. Wang, Z. Wang, W. Yao, G. B. Liu, and H. Y. Yu, Inter-layer coupling in commensurate and incommensurate bilayer structures of transition-metal dichalcogenides, *Phys. Rev. B* **95**, 115429 (2017).
- ¹⁸ F. C. Wu T. Lovorn, E. Tutuc, I. Martin, and A. H. MacDonald, Topological Insulators in Twisted Transition Metal Dichalcogenide Homobilayers, *Phys. Rev. Lett.* **122**, 086402 (2019).
- ¹⁹ D. W. Zhai and W. Yao, Theory of tunable flux lattices in the homobilayer moiré of twisted and uniformly strained transition metal dichalcogenides, *Phys. Rev. Mat* **4**, 094002 (2020).
- ²⁰ H. Y. Yu, M. X. Chen, and W. Yao, Giant magnetic field from moiré induced Berry phase in homobilayer semiconductors, *Natl. Sci. Rev* **7**, 12-20 (2020).
- ²¹ E. McCann and M. Koshino, The electronic properties of bilayer graphene, *Rep. Prog. Phys.* **76**, 5 (2013).
- ²² Q. Niu, M. C. Cheng, B. Wu, D. Xiao, and R. Cheng, *Physical Effects of Geometric Phases* (World Scientific, 2017).
- ²³ A. Böhm, H. Koizumi, Q. Niu, J. Zwanziger, and A. Mostafazadeh, *The Geometric Phase in Quantum Systems* (Springer, 2003).
- ²⁴ R. Shindou and K. I. Imura, Noncommutative geometry and non-Abelian Berry phase in the wave-packet dynamics of Bloch electrons, *Nucl. Phys. B* **720**, 399 (2005).
- ²⁵ D. Culcer, Y. Yao, and Q. Niu, Coherent wave-packet evolution in coupled bands, *Phys. Rev. B*, **72**, 085110 (2005).
- ²⁶ M.-C. Chang and Q. Niu, Berry curvature, orbital moment, and effective quantum theory of electrons in electromagnetic fields, *J. Phys.: Condens. Matter* **20**, 193202 (2008).
- ²⁷ E. V. Gorbar, V. A. Miransky, I. A. Shovkovy, and P. O. Sukhachov, Non-Abelian properties of electron wave packets in the Dirac semimetals A₃Bi (A=Na,K,Rb), *Phys. Rev. B* **98**, 045203 (2018).
- ²⁸ T. Stedman, C. Timm and L. M. Woods, Multiband effects in equations of motion of observables beyond the semiclassical approach, *New J. Phys.* **21**, 103007 (2019).
- ²⁹ K. S. Novoselov, et. al, Unconventional quantum Hall effect and Berry's phase of 2π in bilayer graphene, *Nat. Phys.* **2**, 177 (2006).
- ³⁰ E. McCann and V. I. Fal'ko, Landau-Level Degeneracy and Quantum Hall Effect in a Graphite Bilayer, *Phys. Rev. Lett.* **96**, 086805 (2006).
- ³¹ T. Ohta, A. Bostwick, T. Seyller, K. Horn, and E. Rotenberg, Controlling the Electronic Structure of Bilayer Graphene, *Science* **313**, 951 (2006).
- ³² E. McCann, Asymmetry gap in the electronic band structure of bilayer graphene, *Phys. Rev. B* **74**, 161403(R) (2006).
- ³³ E. V. Castro, et al, Biased Bilayer Graphene: Semiconductor with a Gap Tunable by the Electric Field Effect, *Phys. Rev. Lett.* **99**, 216802 (2007).
- ³⁴ J. B. Oostinga, H. B. Heersche, X. L. Liu, A. F. Morpurgo, and L. M. K. Vandersypen, Gate-induced insulating state in bilayer graphene devices, *Nat. Mater.* **7**, 151 (2008).
- ³⁵ Y. B. Zhang, et al, Direct observation of a widely tunable bandgap in bilayer graphene, *Nature* **459**, 820 (2009).
- ³⁶ L. Yang, J. Deslippe, C. H. Park, M. L. Cohen, and S. G. Louie, Excitonic Effects on the Optical Response of Graphene and Bilayer Graphene, *Phys. Rev. Lett.* **103**, 186802 (2009).
- ³⁷ L. Ju, et al, Topological valley transport at bilayer graphene domain walls, *Nature* **520**, 650 (2015).
- ³⁸ K. Kang, T. Li, E. Sohn, J. Shan, and K. F. Mak, Nonlinear anomalous Hall effect in few-layer WTe₂, *Nat. Mater.* **18**, 324 (2019).
- ³⁹ The nonlinear Hall effect supported by Berry curvature dipoles aims at the higher-order action of an ac electric field on the off-equilibrium distribution where extrinsic scattering plays important roles. It keeps a single band in the active manifold so the remote band effects are well accounted adiabatically, giving rise to the *Abelian* Berry curvature^{40,41}. Here instead we are interested in the non-perturbation action of a dc electric field on intrinsic inter-band transitions within the multiple-band active manifold, where remote band effects are manifested by *non-Abelian* Berry curvatures.
- ⁴⁰ I. Sodemann and L. Fu, Quantum Nonlinear Hall Effect Induced by Berry Curvature Dipole in Time-Reversal Invariant Materials, *Phys. Rev. Lett.* **115**, 216806 (2015).
- ⁴¹ Z. Z. Du, C. M. Wang, S. Li, H.-Z. Lu, and X. C. Xie, Disorder-induced nonlinear Hall effect with time-reversal symmetry, *Nat. Commun.* **10**, 3047 (2019).
- ⁴² The ensemble-averaged velocity \bar{v}_i given in Eq. (3b) though looks similar to the velocity expression of a single wave packet \dot{r} given by the first line of Eq. (1a) in terms of the decomposition into intra-manifold and inter-manifold processes, they are fundamentally different. The velocity in Eq. (1a) is obtained by the full coherent evolution of a single wave packet. Its value at a given instance on which the wave packet has been driven to carry the momentum \mathbf{k} is fully dependent on the non-Markov history of band amplitudes and the Bloch momentum of the wave packet. Henceforth \dot{r} is not fixed by the present \mathbf{k} and \mathbf{E} alone. The ensemble-averaged velocity is obtained from taking into account the Markov decoherence process through the evaluation of the density operator in the steady-state limit at each \mathbf{k} . Therefore, \bar{v}_i is fully determined by \mathbf{k} and \mathbf{E} . The integral in Eq. (3a) for the current arising from an ensemble of wave packets is then well-defined. See more

- details in Ref.¹⁶.
- ⁴³ F. Wilczek and A. Zee, Appearance of gauge structure in simple dynamical systems, Phys. Rev. Lett. **52**, 2111 (1984).
- ⁴⁴ We have shown analytically in Ref.¹⁶ that by taking the dimensionless quantities $|\bar{\mathcal{R}}_{n_R, m_A} \cdot \mathbf{E} / (\varepsilon_{n_R} - \varepsilon_{m_A})|$, where n_R/m_A belong to remote/active bands, as perturbation to the first order, J_R^H reduces to the form with non-Abelian Berry curvature as shown in Eqs. (5) and (6). Since this is a perturbation result, J_R^H of course is expected to be small. Here this anticipation is verified in the numerical calculation.
- ⁴⁵ A. B. Kuzmenko, I. Crassee, D. van der Marel, P. Blake, and K. S. Novoselov, Determination of the gate-tunable band gap and tight-binding parameters in bilayer graphene using infrared spectroscopy, Phys. Rev. B **80**, 165406 (2009).
- ⁴⁶ K. Kechedzhi, V. I. Fal'ko, E. McCann, and B. L. Altshuler, Influence of Trigonal Warping on Interference Effects in Bilayer Graphene, Phys. Rev. Lett. **98**, 176806 (2007).
- ⁴⁷ Usually $r_{c,v}$ is peaked at the Dirac point because the gap size there is the smallest. Nevertheless in Fig. 5(a), with $\gamma_3 = 0$ the Berry connection there vanishes, namely, $[\mathcal{R}_{\mathbf{k}=0}]_{c,v} = 0$. The band structure is dramatically changed by $\gamma_3 \neq 0$ with the trigonal warping effect also visible in $r_{c,v}$. The directionality of \mathbf{E} (here set in the direction of \hat{x}) slightly deviates $r_{c,v}$'s \mathbf{k} -dependence from the symmetry of energy dispersion, as a result of definition of Eq. (9). Noticeably, the anisotropy of energy dispersion with $\gamma_3 \neq 0$ is also accompanied by stronger non-adiabatic intra-manifold transition effects with respect to the same value of gap (see the differences in color bars between Fig. 5(a) and Fig. 5(c)).